Advanced Powder Technology 22 (2011) 115–123

Contents lists available at ScienceDirect

Advanced Powder Technology

journal homepage: www.elsevier.com/locate/apt

Translated paper

Numerical simulation for the transport of solid particles with a vortex ring ☆

Hisanori Yagami [a,*], Tomomi Uchiyama [b]

[a] Management Office for Intellectual Property, Mie University, 1577 Kurimamachiya-cho, Tsu 514-8507, Japan
[b] EcoTopia Science Institute, Nagoya University, Furo-cho, Chikusa-ku, Nagoya 464-8603, Japan

ARTICLE INFO

Article history:
Received 2 September 2010
Accepted 2 September 2010
Available online 21 September 2010

Keywords:
Particle transport
Vortex ring
Numerical simulation
Preferential concentration

ABSTRACT

The objective of this study is to search for the possibility to transport or deliver small solid particles by a vortex ring. The numerical simulation for the motion of a vortex ring and glass particles is performed. At the launch of a vortex ring into quiescent air, spherical particles are arranged on the cross-section of the vortex ring. The cases of the Stokes number St of 0.01 and 1 are simulated by the vortex method. The simulation for St = 0.01 highlights that the vortex ring involves the particles at the launch and that it can transport the particles at a distance of 5.5 times longer than the initial diameter of the vortex ring. The simulation also clarifies the effect of St on the behavior of the vortex ring and the particle motion.

1. Introduction

It is well known that a vortex ring can transport mass and momentum through its convection with the self-induced velocity. The transport ability is so high that it has received much attention. Some applications of vortex ring to convey particles have been reported. Domon et al. [1] conducted an experimental study on the transport of solid particles. In their experiment, a vortex ring was loaded with small resin particles at the launch into still water, and the behavior of the particles transported by the vortex ring was observed. Yanagida et al. [2] proposed an olfactory display method for a virtual reality of the next generation. Scented particles, charged into a vortex ring, were efficiently delivered to a specific user's nose by the convection of the vortex ring through the air. These studies are concerned with the capture and transport of dispersed particles. But the interactions between a vortex ring and particles have scarcely been investigated.

In the authors' prior studies [3,4], the authors simulated the collision of a vortex ring with a cluster of small glass particles to explore the effect on the behavior of the vortex ring and the particle motion. The vortex method for gas-particle two-phase flow, which was developed by one of the authors [5], was employed for the simulation. In the method, the gas vorticity field is discretized by vortex elements, and the behavior of the vortex element is traced with the Lagrangian approach. The method can simulate directly the development of vortical structures, such as the formation and deformation of vortices. The validity and applicability were successfully demonstrated through the various simulations of particle-laden gas flows [6–9].

In this study, the ability of a vortex ring to capture and transport small particles is analyzed with the numerical simulation. At the launch of a vortex ring into quiescent air, spherical glass particles are arranged on the cross-section of the vortex ring. The behavior of the vortex ring and the particle motion are simulated by the authors' vortex method. The Reynolds number of the vortex ring, based on the diameter and the convection velocity, is 2600. It is known that the particle motion around a large-scale eddy can be classified with the Stokes number St, which is defined as the ratio of the particle response time to the characteristic time of the eddy [10]. Considering that St is the dominant parameter for the motion of the particles around the vortex ring, this study simulates the cases of St = 0.01 and 1. The particle diameter for St = 0.01 is 5.25 μm and that for St = 1 is 52.5 μm. The simulation for St = 0.01 demonstrates that the vortex ring captures or entrains the particles at the launch and that it can transport the particles at a distance of 5.5 times longer than the initial diameter of the vortex ring. It also highlights that the vortex ring for St = 1 captures and transports the particles just after the launch and that it hardly transports them. The effect of St on the strength and convection velocity of the vortex ring is also made clear by the simulation.

2. Basic equations

2.1. Assumptions

The following assumptions are employed for the simulation.

(1) The gas is incompressible.
(2) The particle density is much larger than the gas.

☆ Japanese version published in JSPTJ, Vol. 45, No. 12 (2008); English version for APT received on 2 Sept. 2010.

* Corresponding author.
E-mail address: yagami@crc.mie-u.ac.jp (H. Yagami).

0921-8831/$ - see front matter © 2010 The Society of Powder Technology Japan. Published by Elsevier B.V. and The Society of Powder Technology Japan. All rights reserved.
doi:10.1016/j.apt.2010.09.002

Nomenclature

d	particle diameter (m)
D	diameter of vortex ring (m)
$\boldsymbol{f}_D$	drag force acting on particle (N)
$\boldsymbol{F}_D$	force exerted by particle acting on air per unit volume (N/m3)
$\boldsymbol{g}$	gravitational acceleration (m/s^2)
N	number of particles (−)
p	pressure (Pa)
Re	Reynolds number (−)
St	Stokes number = τ_p/τ_g (−)
t	time (s)
t^*	non-dimensional time = tU_c/D_0 (−)
$\boldsymbol{u}$	velocity (m/s)
U_c	convective velocity of vortex ring at $z = 3D_0$ (m/s)
x, y, z	orthogonal coordinates (m)
z_v	axial position of vortex ring (m)
γ	strength of vortex element (m^3/s)
$\boldsymbol{\Gamma}$	circulation (m^2/s)
Δt	time increment = $0.01D_0/U_c$ (s)
ν	kinematic viscosity (m^2/s)
ρ	density (kg/m^3)
σ	core radius of vortex element (m)
τ	characteristic time (s)
$\boldsymbol{\omega}$	vorticity = $\nabla \times u_g$ (1/s)

Superscripts

α	vortex element α
β	vortex element β

Subscripts

0	initial value
g	gas
p	particle
x, y, z	component in direction of x, y or z

(3) The particle has a spherical shape with uniform diameter and density.
(4) The collision between the particles is negligible.

2.2. Governing equations for gas and particle

The conservation equations for the mass and momentum of the gas are expressed as follows under assumption (1):

$$\nabla \cdot \boldsymbol{u}_g = 0 \tag{1}$$

$$\frac{\partial \boldsymbol{u}_g}{\partial t} + (\boldsymbol{u}_g \cdot \nabla)\boldsymbol{u}_g = -\frac{1}{\rho_g}\nabla p + \nu\nabla^2 \boldsymbol{u}_g - \frac{1}{\rho_g}\boldsymbol{F}_D \tag{2}$$

where $\boldsymbol{F}_D$ is the force exerted by the particle acting on the gas per unit volume.

Using assumption (2), the dominant forces on the particle are the drag and gravitational forces, while the virtual mass force, the Basset force and the pressure gradient force are negligible [11]. The lift force is neglected with the reference to the studies simulating the particle motion in a jet [12], a plane wake [13], and mixing layers [11,14]. Consequently, the equation of motion for a particle (mass m) is written as:

$$m\frac{\mathrm{d}\boldsymbol{u}_p}{\mathrm{d}t} = \boldsymbol{f}_D + m\boldsymbol{g} \tag{3}$$

where the drag force $\boldsymbol{f}_D$ is given by the following from assumption (3).

$$\boldsymbol{f}_D = (\pi d^2 \rho_g/8) C_D |\boldsymbol{u}_g - \boldsymbol{u}_p|(\boldsymbol{u}_g - \boldsymbol{u}_p) \tag{4}$$

Here, d is the particle diameter, and the drag coefficient C_D is estimated as [15]:

$$C_D = (24/\mathrm{Re}_p)(1 + 0.15\mathrm{Re}_p^{0.687}) \tag{5}$$

where $\mathrm{Re}_p = d|\boldsymbol{u}_g - \boldsymbol{u}_p|/\nu$.

For the simultaneous calculation of Eqs. (1)–(3), a vortex method is used to solve Eqs. (1) and (2), and the Lagrangian approach is applied to Eq. (3).

2.3. Discretization of vorticity field by vortex element

When taking the curl of Eq. (2) and substituting Eq. (1) into the resultant equation, the vorticity equation for the gas is derived:

$$\frac{D\omega}{Dt} = (\omega \cdot \nabla)\boldsymbol{u}_g + \nu\nabla^2\omega - \frac{1}{\rho_g}\nabla \times \boldsymbol{F}_D \tag{6}$$

where $\boldsymbol{\omega}$ is the vorticity.

The gas velocity $\boldsymbol{u}_g$ at $\boldsymbol{x}$ is given by the Biot–Savart equation.

$$\boldsymbol{u}_g(\boldsymbol{x}) = -\frac{1}{4\pi}\int \frac{(\boldsymbol{x} - \boldsymbol{x}') \times \omega(\boldsymbol{x}')}{|\boldsymbol{x} - \boldsymbol{x}'|^3} dV(\boldsymbol{x}') \tag{7}$$

The gas vorticity field is discretized by vortex elements. A blob model [16] is employed in this study. The vortex element has a cylindrical shape, while the vorticity distribution is spherical with a finite core radius.

When the vortex element α at $\boldsymbol{x}^\alpha$ is supposed to have the core radius σ_α, the vorticity at $\boldsymbol{x}$ induced by the element is expressed as:

$$\omega^\alpha(\boldsymbol{x}) = \frac{\gamma^\alpha}{\sigma_\alpha^3} f\left(\frac{|\boldsymbol{x} - \boldsymbol{x}^\alpha|}{\sigma_\alpha}\right) \tag{8}$$

Here, $f(\varepsilon)$ is the core distribution function, and γ^α is the strength of vortex element expressed as:

$$\gamma^\alpha = \omega^\alpha \delta_\alpha = \Gamma_\alpha \boldsymbol{l}^\alpha \tag{9}$$

where $\boldsymbol{\Gamma}_\alpha$, $\boldsymbol{\delta}_\alpha$ and $\boldsymbol{l}^\alpha$ are the circulation, volume and length vector of the vortex element, respectively. The core distribution function $f(\varepsilon)$ is given by the following equation proposed for single-phase flow [16].

$$f(\varepsilon) = \frac{15}{8\pi(\varepsilon^2 + 1)^{7/2}} \tag{10}$$

2.4. Convection of vortex element and evolution of vortex strength

When the gas vorticity field is discretized into a set of N_v vortex elements, the gas velocity $\boldsymbol{u}_g(\boldsymbol{x})$ is given by the following equation derived from Eqs. (7) and (8).

$$\boldsymbol{u}_g(\boldsymbol{x}) = -\frac{1}{4\pi}\sum_{\alpha=1}^{N_v} \frac{(\boldsymbol{x} - \boldsymbol{x}^\alpha) \times \gamma^\alpha}{|\boldsymbol{x} - \boldsymbol{x}^\alpha|^3} g\left(\frac{|\boldsymbol{x} - \boldsymbol{x}^\alpha|}{\sigma_\alpha}\right) \tag{11}$$

where the function $g(\varepsilon)$ is determined as:

$$g(\varepsilon) = 4\pi\int_0^\varepsilon f(\varsigma)\varsigma^2 d\varsigma \tag{12}$$

The vortex element convects with the gas velocity given by Eq. (11). The Lagrangian approach is used for the calculation.

$$\frac{d\boldsymbol{x}^{\alpha}}{dt} = \boldsymbol{u}_g(\boldsymbol{x}^{\alpha}) \tag{13}$$

Rewriting the vorticity equation, Eq. (6), in the Lagrangian coordinates, the equation is expressed as:

$$\frac{d\omega}{dt} = (\omega \cdot \nabla)\boldsymbol{u}_g + \nu\nabla^2\omega - \frac{1}{\rho_g}\nabla \times \boldsymbol{F}_D \tag{14}$$

It is found from Eq. (14) that the vorticity of vortex element varies with the lapse of time due to the change in the length of vortex element, the viscous diffusion, and the force exerted by the particles. The viscous diffusion is computed by applying the particle strength exchange method [17]. In this case, the substitution of Eqs. (8) and (11) into Eq. (14) yields the time rate of change in the strength of vortex element γ^{α}:

$$\frac{d\gamma^{\alpha}}{dt} = \frac{1}{4\pi}\sum_{\beta=1}^{N_v}\frac{1}{\sigma^3}\left\{-\frac{g(\varsigma)}{\varsigma^3}\gamma^{\alpha}\times\gamma^{\beta} + \frac{1}{\sigma^2}\left[-\frac{1}{\varsigma}\frac{d}{d\varsigma}\left(\frac{g(\varsigma)}{\varsigma^3}\right)\right]\right.$$
$$\left.\times\left[\gamma^{\alpha}\cdot(\boldsymbol{x}^{\alpha}-\boldsymbol{x}^{\beta})\right]\left[(\boldsymbol{x}^{\alpha}-\boldsymbol{x}^{\beta}\times\gamma^{\beta}\right]\right\}\frac{2\nu}{\sigma^2}\sum_{\beta=1}^{N_v}(\delta_{\alpha}\gamma^{\beta}-\delta_{\beta}\gamma^{\alpha})$$
$$\times\eta_{\sigma}(\boldsymbol{x}^{\alpha}-\boldsymbol{x}^{\beta}) \tag{15}$$

where $\zeta = |\boldsymbol{x}^{\alpha}-\boldsymbol{x}^{\beta}|/\sigma$. The second term on the right side of Eq. (15) is the viscous diffusion term. The function $\eta_{\sigma}(\boldsymbol{x})$ is determined as:

$$\eta_{\sigma}(\boldsymbol{x}) = \eta(|\boldsymbol{x}|/\sigma)/\sigma^3 \tag{16}$$

where

$$\eta(\varepsilon) = -\frac{1}{\varepsilon}\frac{d}{d\varepsilon}f(\varepsilon) \tag{17}$$

2.5. Change in strength of vortex element due to particle

When substituting Eq. (6) into an equation, derived from the Reynolds transport theorem and Eq. (1), the time rate of change in the strength of vorticity γ in any volume is obtained:

$$\frac{D\gamma}{Dt} = -\frac{1}{\rho_g}\int(\nabla\times\boldsymbol{F}_D)dV = -\frac{1}{\rho_g}\int(\boldsymbol{n}\times\boldsymbol{F}_D)dS \tag{18}$$

where $\boldsymbol{n}$ is the unit vector normal to the volume surface.

The computational domain is resolved into hexahedral grids, and the time rate of change for γ, $\Delta\gamma/\Delta\boldsymbol{t}$, in each grid is calculated from Eq. (18). As $\boldsymbol{F}_D$ is the reaction of the drag force $\boldsymbol{f}_D$ acting on the particle, $\boldsymbol{F}_D$ value in each grid is computed from $\boldsymbol{f}_D$ acting on the particles in the grid. In the case that the number of vortex elements in a grid is n_v, the change in the strength for each vortex element during $\Delta\boldsymbol{t}$ is supposed to be $\Delta\gamma/n_v$. In the case that there are no vortex elements in the grid, a vortex element with a strength $\Delta\gamma$ is generated at the grid center [5].

3. Simulation conditions

The diameter for vortex ring D and that for vortex core d_v are defined as shown in Fig. 1 (a). As the vorticity takes its maximum value at the center of vortex core, the diameter for the center is measured as D. The distance between the positions where the axial velocity u_{gz} takes the maximum and minimum values is defined as d_v. The initial diameter D_0 is 64 mm, and the initial value for d_v is set at $0.25D_0$. Drawing two closed circuits abcda and abefa on the z–y plane around the vortex ring as shown in Fig. 1(b), the circulation Γ for the vortex ring is estimated by the following equation [18].

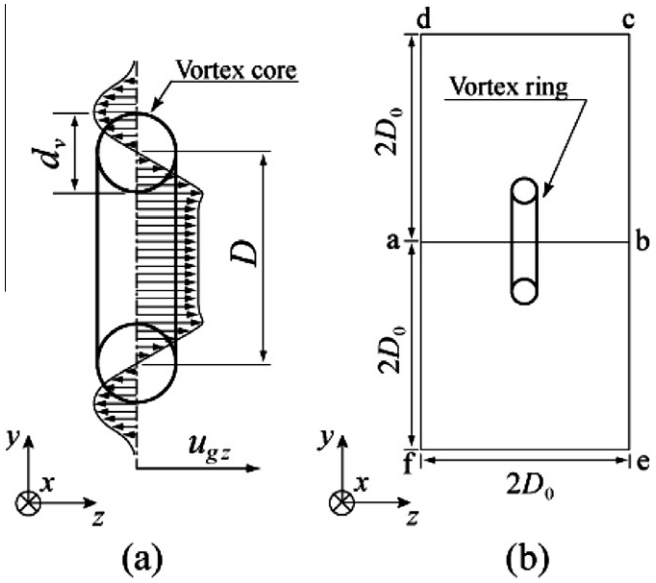

Fig. 1. Definition for properties of vortex ring.

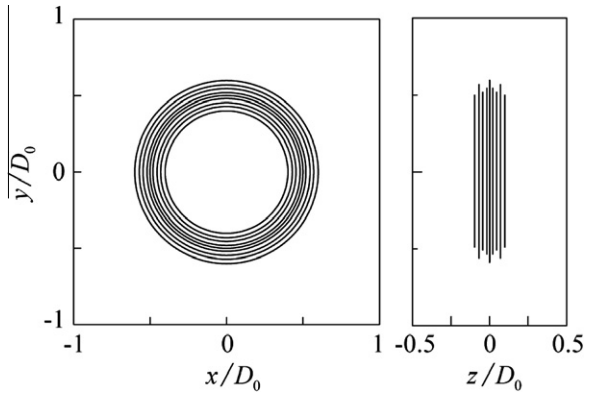

Fig. 2. Vortex ring represented by vortex elements.

$$\Gamma = \frac{1}{2}\left[\int_{\text{abcda}}\boldsymbol{u}_g\cdot d\boldsymbol{s} - \int_{\text{abefa}}\boldsymbol{u}_g\cdot d\boldsymbol{s}\right] \tag{19}$$

The vortex ring is discretized by vortex elements. The arrangement of the vortex element at the initial time $t^* = 0$ is based on the model of Knio and Ghoniem [19] in the same to the authors' prior studies [3,4]. The vortex elements are plotted as the vortex filaments in Fig. 2. The number of vortex elements is 2040. The seventeen vortex elements, representing the cross-section of the vortex core, are connected in the circumferential direction to form the vortex ring. The strength γ_0 for each vortex element at $t^* = 0$ is

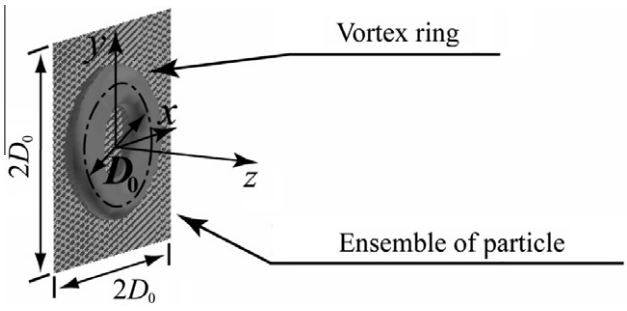

Fig. 3. Initial arrangement for vortex ring and particles.

determined so that the vorticity distribution within the cross-section of the vortex core agrees with the third-order Gaussian curve. The core radius of vortex element σ is set at $0.07D_0$.

Fig. 3 illustrates the arrangement of the vortex ring and the particles at $t^* = 0$. The vortex ring is set at the origin of coordinate. It convects in the z-direction with the self-induced velocity in quiescent air. On the x–y plane at $z = 0$, spherical glass particles with density 2590 kg/m^3 are uniformly distributed within a square area having a side length $2D_0$. The number of particles N_0 is 107 584. The gravitational force is neglected to study the interaction between the vortex ring and the particles. When there are no particles, the Reynolds number for the vortex ring D_0U_0/ν is 2600, where U_0 is the convection velocity at $z = 3D_0$.

Crowe et al. [10] proposed the Stokes number St, which is the ratio of the particle response time $\tau_p = \rho_p d^2/18\rho_g \nu$ to the characteristic time of the gas flow τ_g, as the parameter classifying the particle motion around a large-scale eddy in free turbulent flows.

Estimating the τ_g value as d_v/U_c, the cases of St = 0.01 and 1 are simulated in this study. The particle diameters for St = 0.01 and 1 are 5.25 and 52.5 μm, respectively.The computational region, $3D_0 \times 3D_0 \times 8D_0$, is resolved into $41 \times 41 \times 108$ hexahedral grids to apply Eq. (18). The second-order Adams–Bashforth method is used for the Lagrangian calculation of Eqs. (13) and (15). The time increment Δt is $0.01D_0/U_c$. The vortex element is stretched with its convection, causing the deterioration of the spatial resolution. To maintain the resolution, the vortex element is divided into two

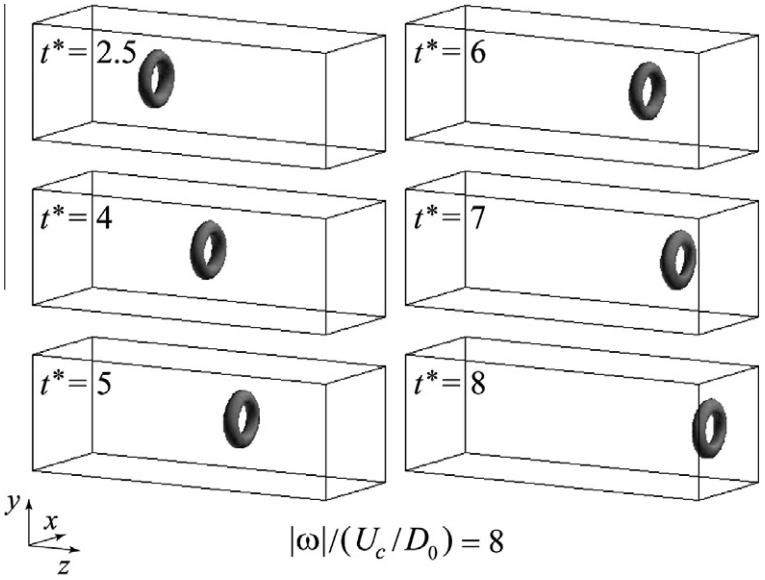

Fig. 4. Convection of vortex ring at particle-free condition.

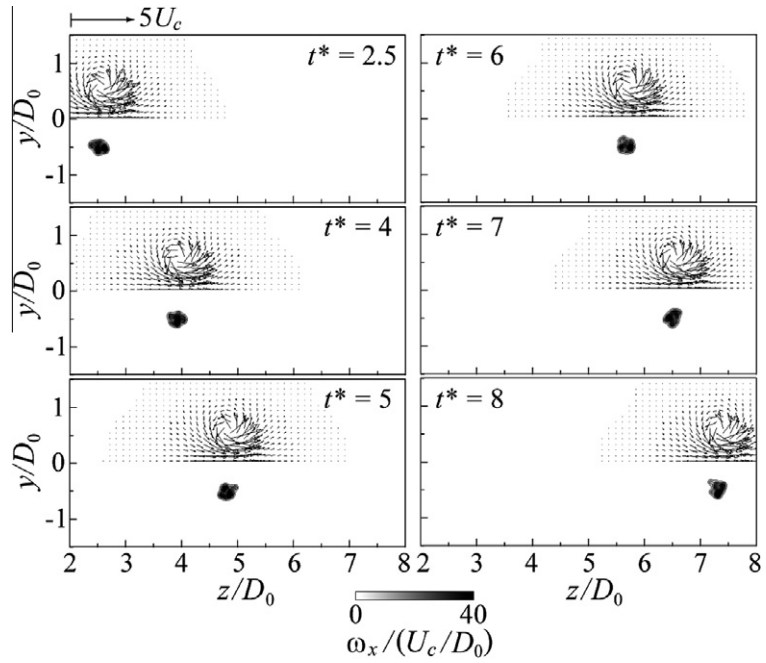

Fig. 5. Air velocity *ug* and velocity component ω_x at particle-free condition (Distributions of $\boldsymbol{u}_g$ and ω_x are plotted at $y > 0$ and $y < 0$, respectively).

vortex elements having the same strength when the strength $|\gamma|$ reaches the twice its initial value $|\gamma_0|$.

4. Results and discussion

4.1. Behavior of vortex ring colliding with no particles

The vortex ring behaves as shown in Fig. 4 when it collides with no particles. The iso-surface for the vorticity of $|\boldsymbol{\omega}|/(U_c/D_0) = 8$ at six time points is presented. The vortex ring convects by the self-induced velocity with maintaining the torus shape.

Fig. 5 shows the distributions for the air velocity and vorticity component ω_x on the z–y plane at the same instant as Fig. 4. The strength for vortex ring decreases with the passage of time. But the decrement is not so remarkable.

4.2. Behavior of vortex ring and particle motion when St = 0.01

In the case of St = 0.01 or $d = 5.25$ μm, the vortex ring and the particles behave as shown in Fig. 6. The particle distribution and the iso-surface for the vorticity of $|\boldsymbol{\omega}|/(U_c/D_0) = 8$ at six time points are presented. At $t^* \leqslant 0.75$, the vortex ring convects in the z-direction with entraining or capturing the particles distributed on the initial plane at $z = 0$. The vortex ring continues to convect with the captured particles at $t^* \geqslant 1.5$. The particles are successfully transported at a distance of $5.5D_0$ when $t^* = 8$. It is found that the vortex ring can capture and transport effectively the particles in the case of St = 0.01. Though the iso-surface for the vorticity still exists at $t^* = 5$ and 8, it is hidden with the surrounding particles.

The particle distribution at the same instant as Fig. 6 is shown in Fig. 7. To grasp easily the distribution on the cross-section of vortex

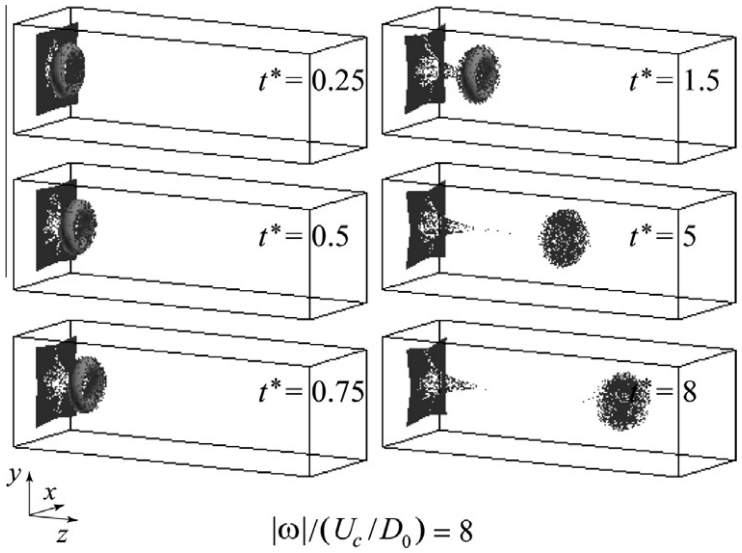

Fig. 6. Convection of vortex ring and particles in case of St = 0.01.

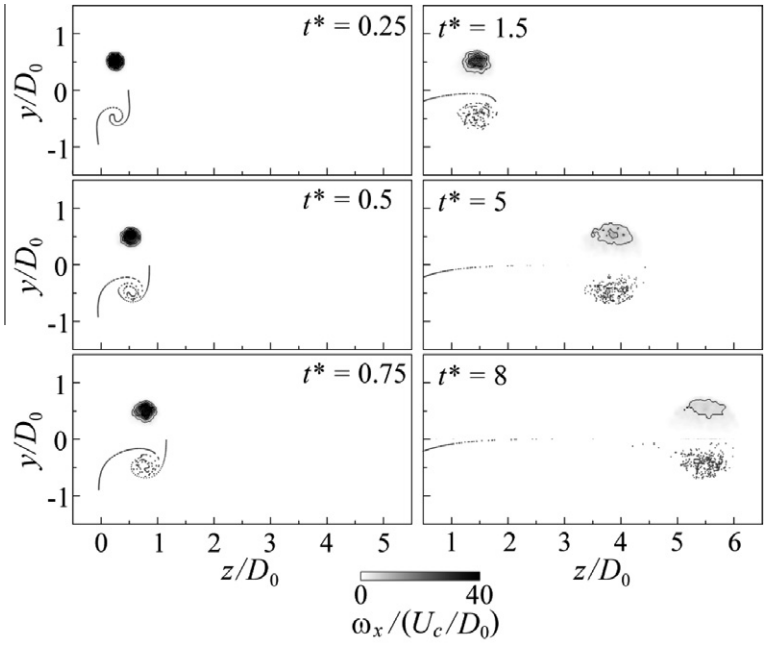

Fig. 7. Distributions for particle and vorticity component ω_x in case of St = 0.01 (ω_x and particles are plotted at $y > 0$ and $y < 0$, respectively).

ring, the particles within the slit region of $-0.1 < x/D_0 < 0.1$ at $y < 0$ are projected onto the z–y plane. The iso-lines for the vorticity component ω_x, which indicate the strength of vortex ring, are superimposed at $y > 0$. Just after the commencement of the convection for the vortex ring $t^* = 0.75$, the particles are entrained or captured into the vortex core on a spiraling path. This is because the particle inertia is so small, and therefore it follows easily the air velocity. The captured particles convect with the vortex ring. The numerical simulation for a plane wake [13] reported that the particles of St = 0.01 are entrained into the large-scale eddies in the wake behind a plate and that they convect with the eddies. The present simulation clarifies that similar phenomena also occur around a vortex ring. The vorticity component $|\omega_x|$ decreases with the lapse of time. At $t^* \geqslant 5$, the vortex core deforms. The vortex strength reduces markedly.

The time variation for the air velocity on the z–y plane is plotted in Fig. 8. The reduction of velocity due to the decrement in the strength of the vortex ring is confirmed.

4.3. Behavior of vortex ring and particle motion when St=1

Fig. 9 shows the particle motion and the behavior of the vortex ring in the case of St = 1 or $d = 52.5$ μm, where the distributions are plotted in the same manner as Fig. 6. At $t^* \leqslant 0.75$, the vortex ring convects in the z-direction with entraining or capturing the particles on the initial plane at $z = 0$. At $t^* \geqslant 1.5$, the captured particles tend to remain behind the vortex ring, and accordingly the number of particles around the vortex ring decreases. Consequently, the particles are transported only just after the commencement of the convection for the vortex ring.

Fig. 10 shows the particle distribution and the vorticity component ω_x at six time points, where the distributions are plotted in the same manner as Fig. 7. Just after the commencement of the convection for the vortex ring $t^* = 0.25$ and 0.5, the particles are rolled up in the z-direction along the inside of vortex ring. At $t^* = 0.75$ and 1.5, the rolled up particles distribute around the vortex ring, forming a dome. This is caused by the fact that the

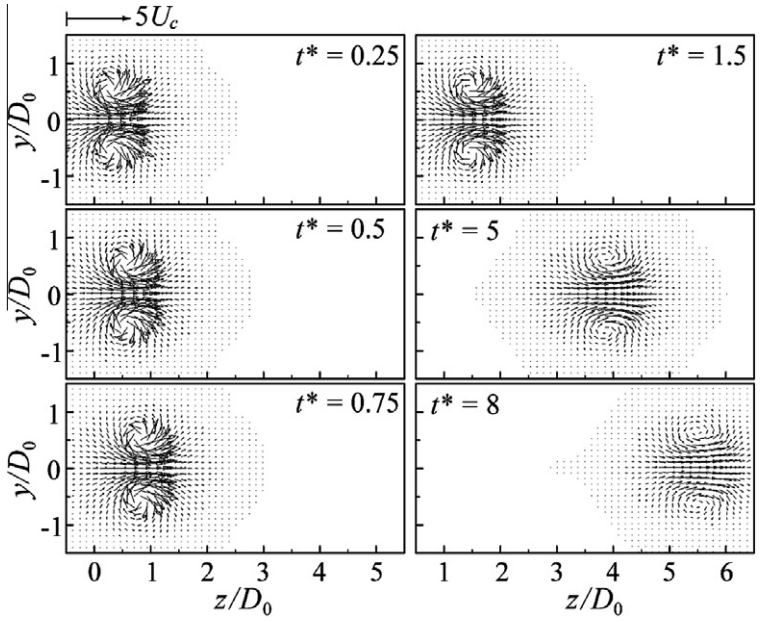

Fig. 8. Air velocity distribution in case of St = 0.01.

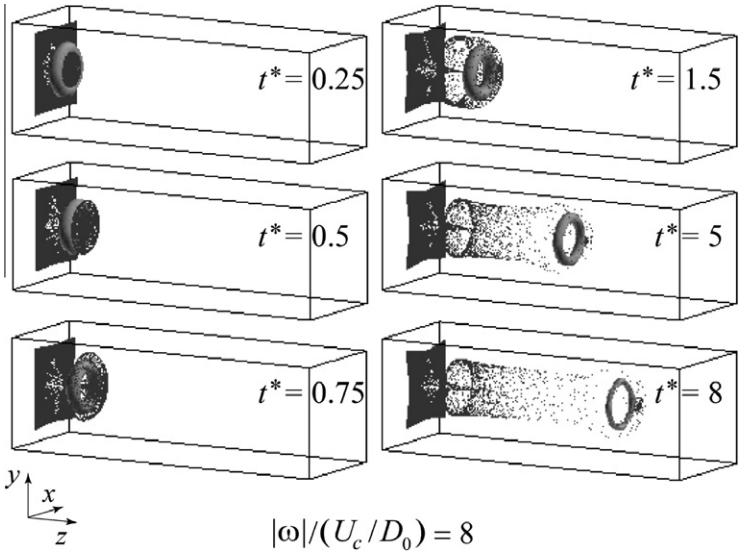

Fig. 9. Convection of vortex ring and particles in case of St = 1.

particles can not fully follow the air velocity in the vortex core, and therefore they are affected by the centrifugal force induced with the vortex ring. Such preferential distribution of the particle of St = 1 on a thin layer around large-scale eddies was investigated by the numerical simulation [13] and experiments [14,20] for various free turbulent flows. And such distribution has been reported by the numerical simulation for the collision between the vortex ring and particles with St = 0.74 in the authors' prior studies [3,4]. The dome elongates in the z-direction with the convection of the vortex ring at $t^* > 1.5$. Since the particles can not fully follow the convection for the vortex ring, the number of particles near the vortex ring decreases with the convection. The strength of vortex ring less decreases when compared with the case of St = 0.01. This is attributable to the fact that no particles are entrained into the vortex core.

The air velocity on the z–y plane distributes as shown in Fig. 11. It reduces with the convection of the vortex element. But the distribution remains almost unaltered.

4.4. Capture and transport of particles

To grasp in detail the ability of the vortex ring to capture and transport the particles, the change in the number of particles near the vortex ring is presented in Fig. 12, where z_v is the axial position of the vortex ring. Counting the particles, of which axial position z satisfies the relation of $z_v\text{-}0.5D_0 \leqslant z \leqslant z_v + 0.5D_0$, the number is

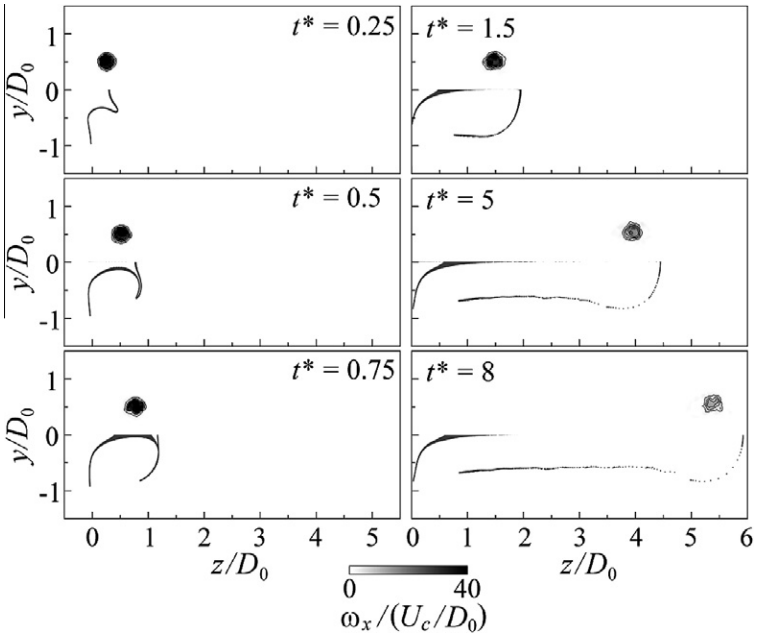

Fig. 10. Distributions for particle and vorticity component ω_x in case of St = 1 (ω_x and particles are plotted at $y > 0$ and $y < 0$, respectively).

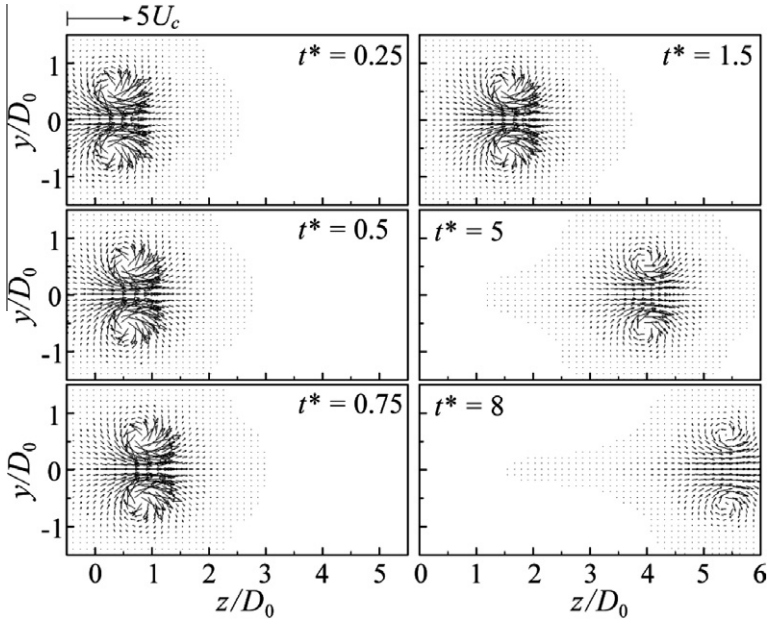

Fig. 11. Air velocity distribution in case of St = 1.

denoted as N. In the case of St = 0.01, N/N_0 takes a constant value 0.41 at $z_v/D_0 \geqslant 0.6$. This suggests that about forty percent of particles are captured by the vortex ring at the commencement of the convection for the vortex ring and that they are successfully transported at a distance of 5.5 times longer than the initial diameter of the vortex ring.

In the case of St = 1, the N value decreases with the convection of the vortex ring at $z_v/D_0 > 3.5$.

The vortex ring scarcely transports the particles at $z_v/D_0 > 3.5$.

4.5. Change in strength of vortex ring

The circulation Γ around the vortex ring calculated from Eq. (19) varies with the passage of time as shown in Fig. 13, where Γ is expressed in the non-dimensional form by using the initial value Γ_0. When the vortex ring is laden with no particles, the reduction of Γ is almost constant. But the laden particles make the reduction larger. The reduction at St = 1 is larger than that at St = 0.01. This is because the number of particles is the same, and accordingly the total particle mass and the force exerted by the particles acting on the vortex ring are larger in the case of St = 1.

The axial velocity of air u_{gz} distributes as shown in Fig. 14, where the distribution on the centerline ($x = y = 0$) at four time points is superimposed. Since the circulation Γ lessens due to the particles as shown in Fig. 13, the maximum value of u_{gz} also decreases. The z value, at which u_{gz} takes its maximum value, indicates the axial position of the vortex ring. The z value reduces due to the laden particles. Therefore, one can grasp the reduction of the convection velocity of the vortex ring.

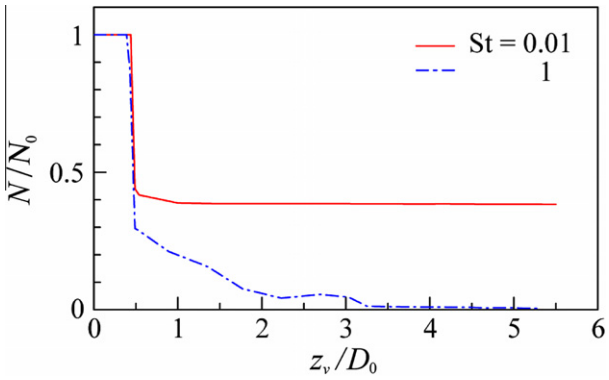

Fig. 12. Axial evolution for number of particles near vortex ring.

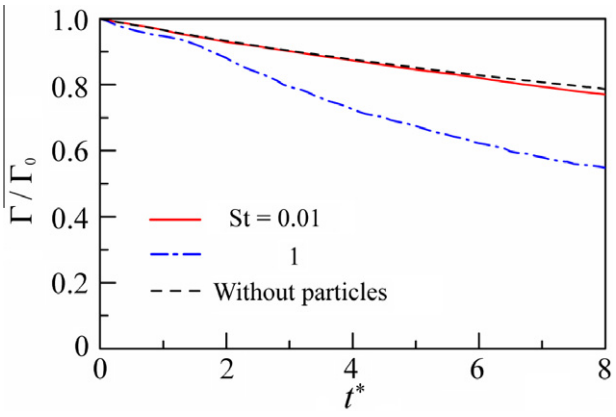

Fig. 13. Time variation for circulation around vortex ring.

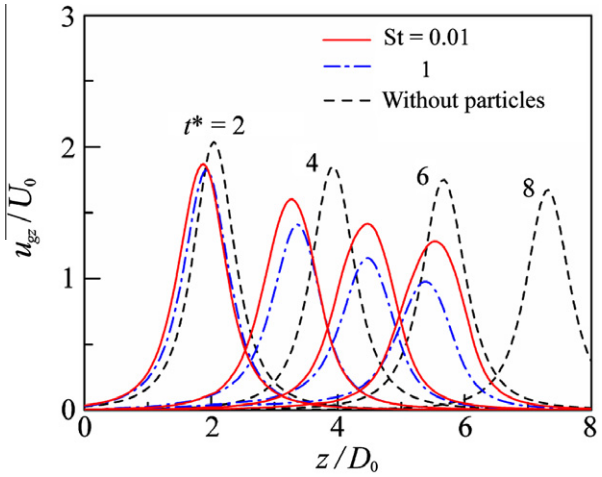

Fig. 14. Air axial velocity on centerline.

5. Conclusions

In order to search for the possibility of a vortex ring to capture and transport small particles, a numerical simulation for the motion of a vortex ring and glass particles is performed. At the launch of a vortex ring into quiescent air, spherical particles are arranged on the cross-section of the vortex ring. The behavior of the vortex ring and the particle motion are simulated numerically by the vortex method. The Reynolds number of vortex ring is 2600, and the cases of the Stokes number St = 0.01 and 1 are computed. The results are summarized as follows:

(1) In the case of St = 0.01, the vortex ring commences to convect with entraining or capturing the particles. The vortex ring continues to convect with the captured particles. It can transport successfully the particles.
(2) In the case of St = 1, the vortex ring commences to convect with capturing a few particles on the initial plane. But the particles tend to remain behind the vortex ring with the convection of the vortex ring, and eventually the particle transportation ceases. The vortex ring hardly transports the particles.
(3) The particles reduce the strength and convection velocity of the vortex ring. The reduction at St = 1 is larger than that at St = 0.01. This is because the number of particles is the same, and accordingly the total particle inertia and the force exerted by the particles acting on the vortex ring are larger in the case of St = 1.

References

[1] K. Domon, O. Ishihara, S. Watanabe, Mass transport by a vortex ring, J. Phys. Soc. Jpn. 69 (1) (2000) 120–123.
[2] Y. Yanagida, S. Kawato, H. Noma, A. Tomono, N. Tesutani, Projection-based olfactory display with nose tracking, in: Proc. IEEE Virtual Reality 2004, Chicago, 2004, pp. 43–50.
[3] T. Uchiyama, H. Yagami, Vortex simulation for the interaction between a vortex ring and solid particles, Proc. 6th Int. Conf. Multiphase Flow, Leipzig (2007). on CD-ROM.
[4] T. Uchiyama, H. Yagami, Numerical simulation for the collision between a vortex ring and solid particles, Powder Technol. 188 (2008) 73–80.
[5] T. Uchiyama, A. Fukase, Three-dimensional vortex method for gas-particle two-phase compound round jet, J. Fluid Eng. 127 (1) (2005) 32–40.
[6] T. Uchiyama, A. Fukase, Three-dimensional vortex simulation of particle-laden air jet, Chem. Eng. Sci. 61 (2006) 1767–1778.
[7] T. Uchiyama, A. Fukase, Vortex simulation of gas-particle two-phase compound round jet, Powder Technol. 165 (2006) 83–91.
[8] H. Yagami, T. Uchiyama, Numerical simulation of particle-laden plane mixing layer by three-dimensional vortex method, JSME Int. J. 49 (4) (2006) 1027–1035.

[9] T. Uchiyama, M. Naruse, Three-dimensional vortex simulation for particulate jet generated by free falling particles, Chem. Eng. Sci. 61 (2006) 1913–1921.
[10] C.T. Crowe, R. Gore, T.R. Troutt, Particle dispersion by coherent structures in free shear flows, Particle Sci. Technol. J. 3 (1985) 149–158.
[11] R. Chein, J.N. Chung, Effects of vortex pairing on particle dispersion in turbulent shear flows, Int. J. Multiphase Flow 13 (6) (1987) 785–802.
[12] J.N. Chung, T.R. Troutt, Simulation of particle dispersion in an axisymmetric jet, J. Fluid Mech. 186 (1988) 199–222.
[13] L. Tang, F. Wen, Y. Yang, C.T. Crowe, J.N. Chung, R. Troutt, Self-organizing particle dispersion mechanism in a plane wake, Phys. Fluids A 4 (10) (1992) 2244–2251.
[14] F. Wen, N. Kamalu, J.N. Chung, C.T. Crowe, R. Troutt, Particle dispersion by vortex structures in plane mixing layers, J. Fluid Eng. 114 (1992) 657–666.
[15] L. Schiller, A.Z. Naumann, Űber die grundlegenden Berechnungen bei der Schwerkraftaufbereitung, Z. Vereines Deutscher Inge. 77 (1933) 318–321.
[16] G.S. Winckelmans, A. Leonard, Contribution to vortex particle methods for the computation of three-dimensional incompressible unsteady flows, J. Comput. Phys. 109 (1993) 247–273.
[17] P. Degond, S. Mas-Gallic, The weighted particle method for convection-diffusion equations, Math. Comput. 53 (1989) 485–507.
[18] J.H. Arakeri, D. Das, A. Krothapalli, L. Lourenco, Vortex ring formation at the open end of a shock tube: a particle image velocimetry study, Phys. Fluids 16 (4) (2004) 1008–1019.
[19] O.M. Knio, A.F. Ghoniem, Numerical study of a three-dimensional vortex method, J. Comput. Phys. 86 (1990) 75–106.
[20] Y. Yang, C.T. Crowe, J.N. Chung, T.R. Troutt, Int. J. Multiphase Flow 26 (2000) 1583–1607.